ADVANCES IN ATMOSPHERIC SCIENCES, VOL. 37, NOVEMBER 2020, 1149–1163

• **Original Paper** •

Combined Impacts of Warm Central Equatorial Pacific Sea Surface Temperatures and Anthropogenic Warming on the 2019 Severe Drought in East China

Shuangmei MA[1], Congwen ZHU[*1], and Juan LIU[2]

[1]*State Key Laboratory of Severe Weather (LASW) and Institute of Climate System, Chinese Academy of Meteorological Sciences, Beijing* 100081, *China*

[2]*Meteorological Service Center of Zhejiang, Hangzhou* 310016, *China*

(Received 16 April 2020; revised 23 July 2020; accepted 24 July 2020)

ABSTRACT

A severe drought occurred in East China (EC) from August to October 2019 against a background of long-term significant warming and caused widespread impacts on agriculture and society, emphasizing the urgent need to understand the mechanism responsible for this drought and its linkage to global warming. Our results show that the warm central equatorial Pacific (CEP) sea surface temperature (SST) and anthropogenic warming were possibly responsible for this drought event. The warm CEP SST anomaly resulted in an anomalous cyclone over the western North Pacific, where enhanced northerly winds in the northwestern sector led to decreased water vapor transport from the South China Sea and enhanced descending air motion, preventing local convection and favoring a precipitation deficiency over EC. Model simulations in the Community Earth System Model Large Ensemble Project confirmed the physical connection between the warm CEP SST anomaly and the drought in EC. The extremely warm CEP SST from August to October 2019, which was largely the result of natural internal variability, played a crucial role in the simultaneous severe drought in EC. The model simulations showed that anthropogenic warming has greatly increased the frequency of extreme droughts in EC. They indicated an approximate twofold increase in extremely low rainfall events, high temperature events, and concurrently dry and hot events analogous to the event in 2019. Therefore, the persistent severe drought over EC in 2019 can be attributed to the combined impacts of warm CEP SST and anthropogenic warming.

Key words: drought, East China, central equatorial Pacific, SST, global warming, model simulations

Citation: Ma, S. M., C. W. Zhu, and J. Liu, 2020: Combined impacts of warm central equatorial Pacific sea surface temperatures and anthropogenic warming on the 2019 severe drought in East China. *Adv. Atmos. Sci.*, **37**(11), 1149–1163, https://doi.org/10.1007/s00376-020-0077-8.

Article Highlights:

- In August–October 2019, East China experienced severe drought, with the lowest precipitation and highest temperature since 1960.
- Drought was naturally driven by the extremely warm CEP SST.
- Global warming has enhanced the probability of severe drought.

1. Introduction

Large-scale persistent drought can cause significant water shortages, economic losses, and adverse social consequences, with far-reaching impacts on the increasingly globalized world (Sternberg, 2011). Over the past decade, record-breaking extreme drought events have occurred more frequently (Lewis et al., 2011; Coumou and Rahmstorf, 2012; Lott et al., 2013; Williams et al., 2015; Ma et al., 2017; Li et al., 2018; Zeng et al., 2019), which has triggered intensive discussions on whether these droughts are related to global warming (Coumou and Rahmstorf, 2012; Dai, 2013; Trenberth et al., 2014; Williams et al., 2015; Huang et al., 2016; Ma et al., 2017; Hoell et al., 2019). It has been suggested that the intensity and duration of droughts have been enhanced due to the increased surface drying and evaporation under global warming (Trenberth, 2011; Huang et al., 2016). While global warming may not cause droughts directly, when droughts occur, they are increasingly likely to exhibit more rapid onsets and

* Corresponding author: Congwen ZHU
Email: zhucw@cma.gov.cn

to be more intense as a result of global warming (Trenberth et al., 2014). In fact, accurate attribution of a drought requires accounting for the impacts of natural variability, such as the El Niño–Southern Oscillation (ENSO), Pacific Decadal Oscillation, and North Atlantic Oscillation (NAO) (Dai, 2013; Trenberth et al., 2014, 2015). Anthropogenic warming has substantially increased the overall likelihood of some regionally extreme droughts beyond the impacts of natural variability (Lott et al., 2013; Williams et al., 2015; Ma et al., 2017; Hoell et al., 2019).

China is a drought-prone country that is sensitive to global warming (Yang et al., 2012; Feng et al., 2014; Wang et al., 2015; Li et al., 2018; Zhang et al., 2018; Zeng et al., 2019). Droughts in China have occurred more frequently and severely, with longer durations and larger affected areas, under global warming (Yu et al., 2014). Most areas of the country are projected to become drier as a consequence of increasing evaporation, and extreme droughts will increase dramatically in the future warming climate (Wang and Chen, 2014). The occurrence of droughts in China is also closely linked to other factors. It has been demonstrated that the decline in Barents Sea ice in spring can enhance hot drought events in summer over northeastern China (Li et al., 2018). The atmospheric circulation anomalies induced by remote forcing from the tropical Pacific and North Atlantic oceans provide important contributions to severe droughts in China (Zhang et al., 2013; Feng et al., 2014; Wang et al., 2015). ENSO, one of the most powerful modes of climate variability that influence the world climate, has been extensively demonstrated to exert significant impacts on climate over China (e.g., Ashok et al., 2007; Feng et al., 2016; Yu et al., 2017; Ren et al., 2018; Li et al., 2019; Gao et al., 2020; Wang et al., 2020). Different ENSO phases yield pronounced anomalous patterns of seasonal precipitation and circulation in China, and the relationship between ENSO and precipitation in China is strongly dependent on the type of ENSO event (Ashok et al., 2007; Feng and Li, 2011; Zhang et al., 2011; 2013; 2014; Yuan and Yang, 2012; Feng et al., 2016; 2017; Li et al., 2019). Additionally, the phase transition from La Niña to El Niño is one of the important precursors of prolonged spring–summer droughts in northern China (Zhang et al., 2018). Moreover, the upstream quasi-stationary wave pattern strengthened by land–atmosphere coupling provided an important contribution to the persistent drought in Northeast China from spring to summer of 2017 (Zeng et al., 2019).

The middle and lower reaches of the Yangtze River constitute a developed economic zone in East China (EC), where frequent droughts have occurred in recent decades (Wu et al., 2006; Yang et al., 2013; Zhang et al., 2014, 2016). Considerable effort has been made to understand the factors influencing EC droughts (e.g., Wu et al., 2006; Sun and Yang, 2012; Jin et al., 2013; Lu et al., 2014; Feng et al., 2016 Huang et al., 2019). Droughts in EC are likely triggered by El Niño Modoki-like sea surface temperature (SST) anomalies (Dai, 2011; Feng and Li, 2011; Zhang et al., 2011; 2013; 2014; Feng et al., 2016; Zhang and Zhou, 2015; Li et al., 2019) and by a positive NAO phase (Sun and Yang, 2012). Drought magnitudes in this region are anticipated to shift from moderate and severe in the past to extreme and exceptional in the future (Sun et al., 2019). Previous studies have significantly improved our understanding of EC droughts. However, few attribution studies have been conducted with respect to extreme drought events in EC.

In August–October 2019, this region experienced the most severe meteorological drought of the past four decades, characterized by a long duration and persistent high temperatures. This drought devastated crops across more than 2.3 million hectares of farmland and caused direct economic damage that amounted to greater than US$ 2.1 billion (http://society.people.com.cn/n1/2019/1106/c1008-31439555.html). Whether severe droughts of this type are likely to increase under anthropogenic global warming is of great concern for both the public and policymakers. Thus, this study aims to understand the possible mechanisms responsible for this most severe EC drought and to further explore its linkage with natural climate variability and anthropogenic global warming.

2. Data and methods

2.1. *Data description*

A total of 2474 in-situ daily precipitation and surface air temperature (SAT) datasets covering the period 1960–2019 were collected from the National Meteorological Information Center of the China Meteorological Administration (http://cdc.nmic.cn/home.do). Data were interpolated to a 0.5° × 0.5° grid using iterative improvement objective analysis with a search radius of 3°, 2°, 1°, 0.5°, respectively, using the "obj_anal_ic_Wrap" function in the NCAR command language (www.ncl.ucar.edu/Document/Functions/Contributed/obj_anal_ic_Wrap.shtml). The monthly reanalyses of atmospheric components were derived from the Japanese 55-year reanalysis (JRA-55), with a horizontal resolution of 1.25° × 1.25° (Kobayashi et al., 2015). Variables included surface pressure, meridional and zonal winds, pressure velocity, and specific humidity. Global monthly SSTs with a horizontal resolution of 2° × 2° were taken from the National Oceanic and Atmospheric Administration Extended Reconstructed SST dataset, version 5 (Huang et al., 2017).

To understand the potential contribution of anthropogenic forcing to seasonal extreme EC droughts, simulations from the Community Earth System Model Large Ensemble (CESM-LE) datasets were used. By simulating climate trajectories over the period 1920–2100 multiple times with small atmospheric initialization differences, but using the same model and external forcing, the CESM-LE project provides a comprehensive resource for studying climate change in the presence of internal climate variability (Kay et al., 2015). There are 40-member ensembles of fully coupled simulations for the period 1920–2100 included in the CESM-LE project. All CESM-LE simulations use the Community

Earth System Model, version 1, with the Community Atmosphere Model, version 5 (CESM1-CAM5). CESM1-CAM5 consists of coupled atmosphere, ocean, land, and sea-ice component models. Here, the outputs from fully coupled preindustrial control (PIC) simulations over 1800 years and historical climate simulations (hereafter "All-forcing") over the period 1920–2019 were used. The All-forcing simulations include both anthropogenic and natural forcing agents from approximately 1850 to the present. The PIC run has constant forcing, set at 1850 levels, and thus enables assessment of internal climate variabilities in the absence of climate change.

2.2. *Methods*

We adopted the generalized extreme value (GEV) distribution to fit the August–October distributions of climate variables and to estimate the corresponding return periods exceeding the year 2019. The least-squares linear regression method was used to estimate the linear trends in climate variables. The climatological base period was defined as 1960–2019. The statistical significances of the trends and the correlation coefficients were calculated using a two-tailed Student's *t*-test.

To quantify the contribution of anthropogenic global warming to the frequency of extreme EC droughts, based on the method of Swain et al. (2018), we calculated percentage changes in the frequency F of extreme EC drought events with the return intervals for the observed 2019 August–October drought in the All-forcing simulations relative to the PIC simulations:

$$\Delta F_{\mathrm{All}} = \frac{F_{\mathrm{All}} - F_{\mathrm{PIC}}}{F_{\mathrm{PIC}}} .$$

Corresponding significances were examined by comparing the frequencies of the extreme EC drought events in the All-forcing simulations with the resampled (bootstrapped) frequencies in the PIC simulations. An F_{All} value falling outside the sampled range of F_{PIC} variability with 90% confidence indicated that an anthropogenic climate change signal was statistically significant. Meanwhile, the 5%–95% uncertainty range of ΔF_{All} was also estimated using the bootstrap resampling method, and the corresponding best estimates were approximated based on the median.

3. Results

3.1. *Characteristics of the drought event over EC in 2019*

The spatial pattern of anomalous precipitation and SATs from August to October in 2019 over EC (Fig. 1) shows a rainfall anomaly of less than −180 mm and a warm SAT anomaly of 1.8°C (Figs. 1a and b), indicating the concurrence of a strong precipitation deficiency and a high-temperature event in 2019. Most stations over the middle and lower reaches of the Yangtze River experienced extremely low precipitation and high temperatures, which broke records since 1960 at many stations. To understand the general variability in SATs and precipitation in EC, the time series of EC area-averaged precipitation and SAT anomalies from 1960 to 2019 were calculated, and they are shown in Figs. 1c and d. EC precipitation and SATs showed substantial interannual variability. In terms of the area-mean precipitation deficit, it was clear that the EC drought from August to October in 2019 was unprecedently severe, with 144 mm less precipitation than normal and a return period of 94 years (Fig. 1c). The concurrent high temperature was ranked the highest since at least 1960, with a warm anomaly of 1.8°C and a return period of 65 years. Although the EC area-mean August–October precipitation levels showed a slight decreasing trend from 1960 to 2019, this trend was not statistically significant and was considered negligible. At the same time, the EC area-mean August–October SAT exhibited a significant warming trend of 0.86°C (60 yr)$^{-1}$.

To document the atmospheric circulation patterns related to the EC drought from August to October in 2019, the corresponding anomalous circulations are illustrated in Fig. 2 and Fig. 3. In the climatological August–October period, a moisture transport branch from the South China Sea, carried by southeasterly winds, supplied precipitation over EC (Fig. 2a). However, in August–October 2019, a strong cyclonic anomaly occurred over the western North Pacific (WNP), and two strong anticyclonic anomalies appeared over the regions to the east of Japan and in the Bay of Bengal (Fig. 2b). The northeasterly wind anomalies on the northwestern side of the anomalous WNP cyclone occurred over EC, and southwestward moisture transport anomalies prevailed over EC (Fig. 2c). These simultaneous anomalous circulation patterns from the 2019 EC drought were similar to the composite structures associated with the El Niño Modoki, also known as the central Pacific El Niño (Zhang et al. 2011, 2014). Consequently, the precipitable water levels in EC were much lower than normal and were not favorable for producing precipitation in EC. The anomalous water vapor transport partly contributed to the EC precipitation deficiency from August to October 2019.

Vertical motion is another important factor affecting the precipitation and SAT anomalies. Figure 3 shows the zonal– and meridional–vertical circulation composite of anomalous winds and pressure velocities in 2019 averaged over EC from August to October. It is noted that, as a result of cold–dry moist enthalpy advection associated with the northerly component of the western flank of the WNP cyclonic anomalies (Ham et al., 2007; Wu et al., 2017), extremely anomalous downdrafts predominated in the troposphere over EC. The enhanced descending motion prevented convection and precipitation and increased solar radiation heating at the surface (Fig. 3c); its associated adiabatic warming facilitated higher surface temperatures and maintained a local anticyclone. Therefore, the co-occurrence of severe drought and high temperature in EC from August to October 2019 was directly caused by

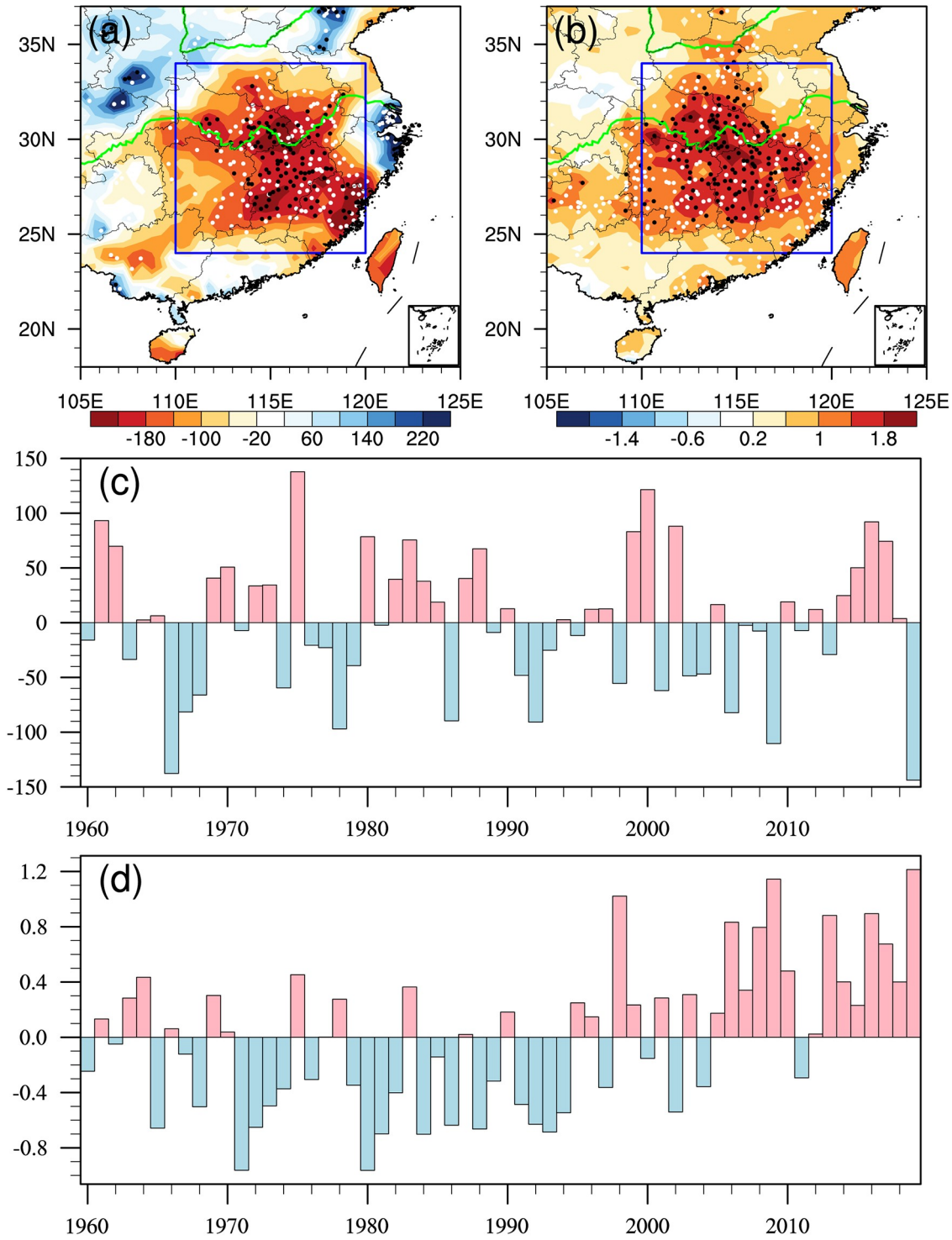

Fig. 1. (a) Precipitation anomalies (unit: mm) and (b) SAT anomalies (unit: °C) from August to October of 2019 compared to those from 1960 to 2019. White and black dots identify stations where August–October precipitation (SAT) anomalies in 2019 were below (exceeded) the 5th (95th) percentile threshold and broke the lowest precipitation (highest SAT) record since 1960, respectively. (c, d) Time series of August–October (c) precipitation anomalies (unit: mm) and (d) SAT anomalies (unit: °C) averaged over EC [indicated by the blue rectangular box bounded by (24°–34°N, 110°–120°E) in (a, b)].

strengthened air descent and reduced moisture transport from the South China Sea, induced by the anomalous NWP cyclone.

3.2. *Linkage with El Niño Modoki-like SST anomalies*

The previous results imply that the local factors that facilitated the severe drought in EC from August to October

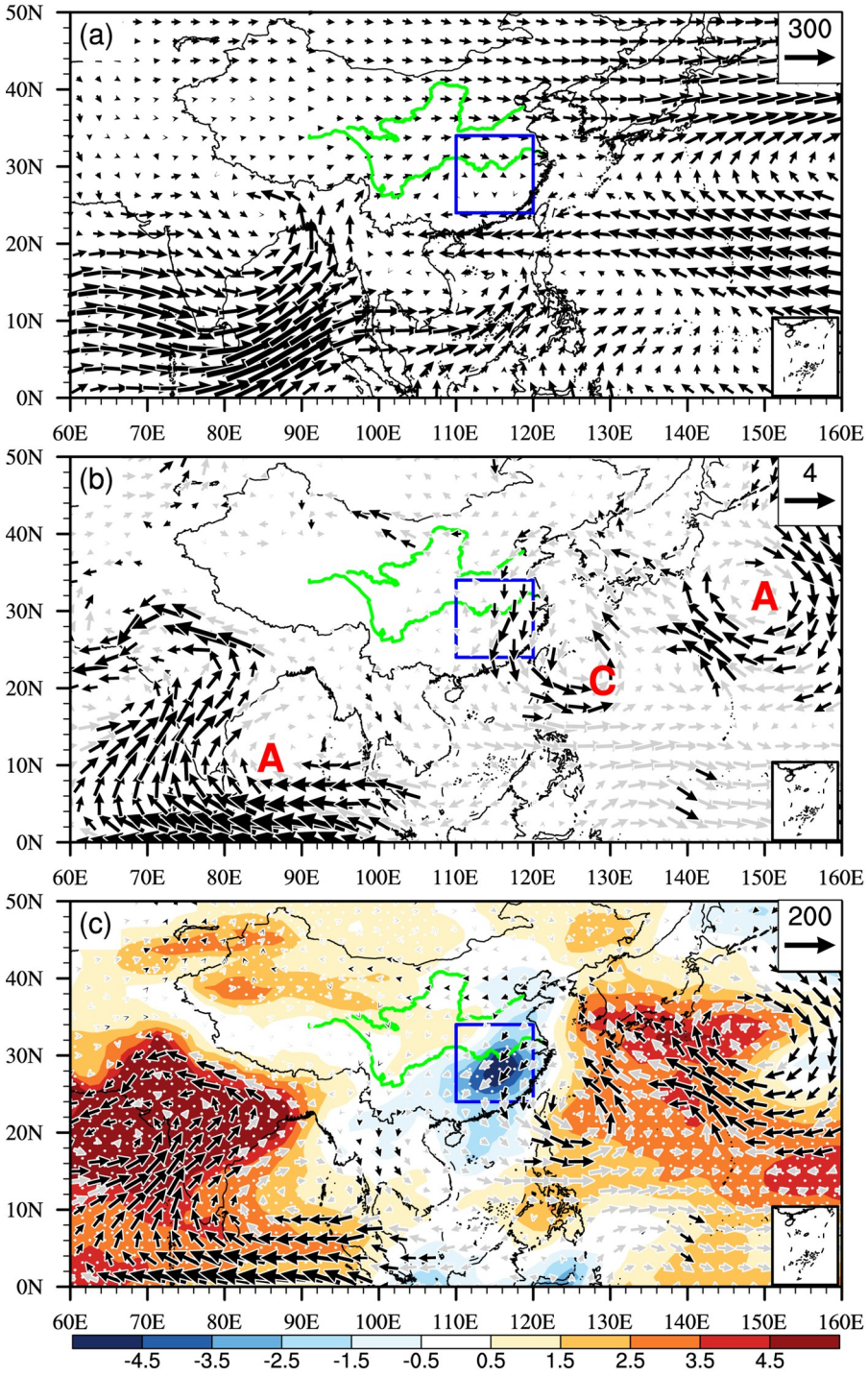

Fig. 2. (a) August–October mean climatology of vertically integrated water vapor transport (units: kg m^{-1} s^{-1}), (b) wind anomalies at 850 hPa (units: m s^{-1}) and (c) vertically integrated water vapor transport anomalies (vectors; units: kg m^{-1} s^{-1}) and water vapor anomalies (shading; units: kg m^{-2}) from August to October of 2019. The letters A and C in (b) mark the centers of anomalous anticyclones and cyclones, respectively. The blue boxes indicate the EC region. Vectors in (b, c) are shown in black where the values fall outside the 5th–95th percentile range in at least one direction. Shading in (c) is stippled by white dots where the values fall outside the 5th–95th percentile range.

2019 were associated with an extensively anomalous cyclone over the NWP. However, the atmospheric circulation regime responsible for the local circulation anomalies over EC deserves further investigation. A number of studies have demonstrated that the atmospheric circulation anomaly responsible for drought in EC is possibly a response to the

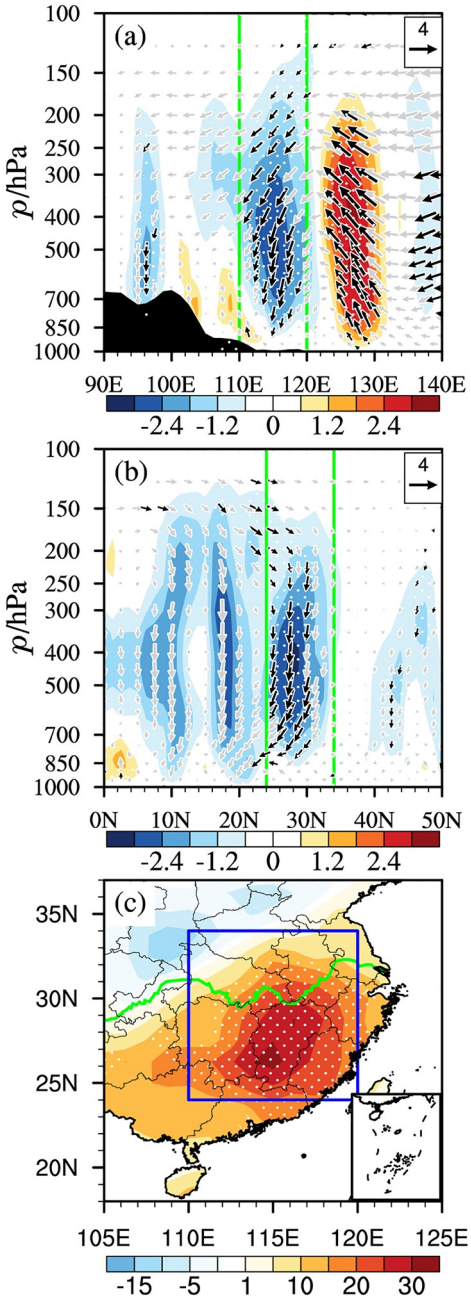

Fig. 3. August–October 2019 anomalies of (a) zonal–vertical circulation [vectors indicate a composite of zonal winds (units: m s^{-1}) and sign-reversed pressure velocities (units: 10^{-2} Pa s^{-1})] averaged over 24°–34°N, and (b) meridional–vertical circulation [vectors indicate a composite of meridional winds (units: m s^{-1}) and sign-reversed pressure velocities (units: 10^{-2} Pa s^{-1})] averaged over 110°–120°E. Shading indicates the sign-reversed pressure velocity (units: 10^{-2} Pa s^{-1}) and is stippled by white dots when the values fall outside the 5th–95th percentile range. Vectors are shown in black when they fall outside of the 5th–95th percentile range in at least one direction. The green lines indicate the EC region, while the black filled areas denote topography. (c) August–October 2019 anomalies (units: W m^{-2}) in the downward solar radiation flux reaching the Earth's surface, shown stippled by white dots when anomalies fall outside the 5th–95th percentile range.

SST anomalies in tropical oceans, especially those strongly linked to the ENSO phenomenon (Dai, 2011, 2013; Feng and Li, 2011; Zhang et al., 2011, 2013, 2014, 2015, 2018; Jin et al., 2013; Wang et al., 2015; Feng et al., 2014, 2016; Ma et al., 2017). To investigate the connection between SST anomalies and EC droughts, we calculated the August–October SST anomalies that were linearly congruent with the interannual variability of EC precipitation by regressing the SST anomalies onto the sign-reversed detrended EC area-mean precipitation from 1960 to 2019. The regression map between EC area-mean precipitation and SST revealed that the most obvious SST anomalies closely linked to EC precipitation variability were mainly centered on the tropical Pacific. A decrease in August–October EC area-mean precipitation corresponded to a tripole pattern of SST anomalies over the tropical Pacific. The significant warm anomalies in the central equatorial Pacific (CEP) were flanked by cold anomalies in the western and eastern equatorial Pacific and extended northeastward to the eastern extratropical Pacific (Fig. 4a), resembling the anomalous SST pattern during El Niño Modoki (Ashok et al., 2007). This indicates that when the tropical Pacific SST exhibits an El Niño Modoki-like anomaly, EC experiences a precipitation deficit, consistent with previous studies (Feng and Li, 2011; Zhang et al., 2011, 2014; Feng et al., 2016). During the severe drought in August–October 2019, extremely warm SST anomalies prevailed over the CEP, while cold SST anomalies appeared over the western and eastern equatorial Pacific (Fig. 4b). This implies that the warm CEP SST anomaly may have played an important role in the anomalous circulation associated with the severe EC drought from August to October 2019.

To explore the possible effects of the El Niño Modoki-like SST anomaly on the EC drought, regression maps of the atmospheric circulation patterns in August–October against the standardized El Niño Modoki Index [EMI, shown in Fig. 4c and defined using the method of Ashok et al. (2007)] from 1960 to 2019 are shown in Fig. 5. Warm conditions over the CEP are associated with significant cyclonic circulation anomalies in the lower troposphere over the WNP (Fig. 5a). The significant northerly wind anomalies on the west side of the anomalous cyclone over the WNP reduce the northward water vapor transport from the South China Sea to EC, leading to an apparent anomalous southward integrated vapor transport and significant negative integrated moisture in EC. The anomalous cyclone over the WNP is not favorable for the accumulation of moisture in EC and thus plays an important role in the induction of precipitation deficiencies in EC, which is followed by drought initiation. Furthermore, a well-organized anomalous local Hadley circulation exists, with a significant anomalous ascent over the CEP and a significant anomalous descent in EC stretching from the South China Sea to North China. This anomalous meridional circulation strengthens the local Hadley circulation over East Asia, and the resulting strongly descending anomalies in EC favor precipitation deficien-

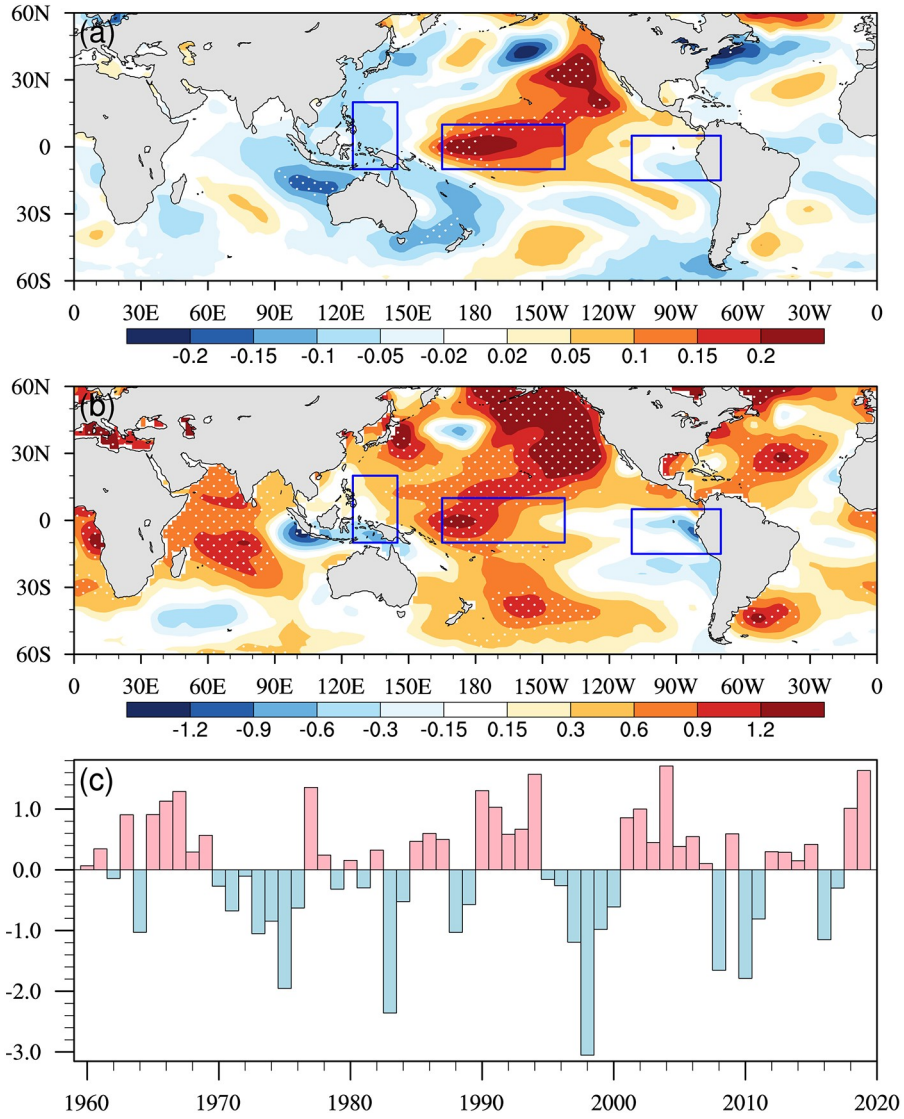

Fig. 4. (a) Linear regression of SST anomalies on the standardized anomalies of the sign-reversed detrended EC area-mean precipitation from August to October of 1960–2019. Stippling indicates significance at the 99% confidence. (b) August–October mean SST anomalies for 2019. Stippling indicates anomalies falling outside the 5th–95th percentile range. The blue rectangular boxes in (a, b) indicate the areas used to calculate the EMI. (c) Time series of the standardized anomalies of August–October mean EMI from 1960 to 2019.

cies, thus intensifying the severity of EC droughts. These anomalous atmospheric circulations associated with El Niño Modoki-like SST anomalies were in good agreement with those observed in 2019 (Fig. 2 and Fig. 3). These similarities suggest that the El Niño Modoki-like tropical Pacific SST anomaly may have been a key external forcing responsible for the severe drought over EC in 2019.

A scatter diagram further confirms the linear linkage between the drought in EC and the El Niño Modoki-like SST anomaly (Fig. 6). As a response to the El Niño Modoki-like SST anomaly, the EC area-mean northerly wind at 850 hPa and the descent at 500 hPa strengthened significantly, while precipitable water and precipitation decreased significantly. The EMI anomaly in 2019 was ranked the second highest since 1960, occurring synchronously with the fourth strongest northerly wind anomaly at 850 hPa, the fifth lowest precipitable water and second strongest descending anomaly at 500 hPa, and the lowest precipitation in EC since 1960. Therefore, the El Niño Modoki-like SST anomaly can be regarded as an important external forcing responsible for the EC drought and its relevant atmospheric circulation anomalies. The strong warm CEP SST anomaly in 2019 was favorable for the occurrence of the most severe precipitation deficiency event in EC.

The above results clearly indicate that the El Niño Modoki-like SST anomaly can affect EC climate by inducing a cyclonic circulation over the NWP. To substantiate the physical connection between El Niño Modoki-like SST anom-

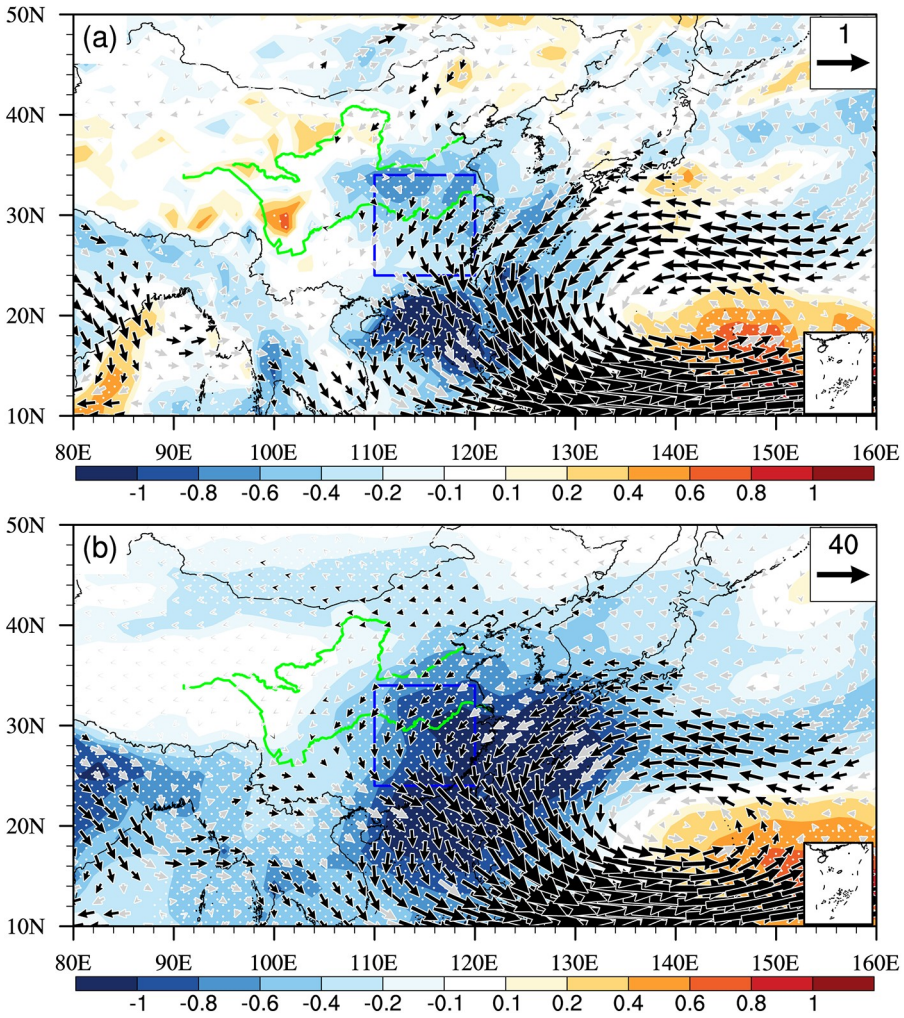

Fig. 5. Atmospheric circulation anomalies linked to the EMI. Linear regression of August–October mean (a) sign-reversed pressure velocity at 500 hPa (shading; units: 10^{-2} Pa s^{-1}) and horizonal wind at 850 hPa (vectors; units: m s^{-1}), and (b) vertically integrated water vapor (shading; units: kg m^{-2}) and water vapor transport (vectors; units: kg m^{-1} s^{-1}) with respect to the detrended standardized EMI from 1960 to 2019. Shading is stippled by white dots when they are significant at the 99% confidence level, and vectors are shown as black when they are significant at the 99% confidence level in at least one direction.

alies and EC droughts, the anomalous SSTs and atmospheric circulations during extreme EC drought years, with a 94-year return interval analogous to that of the observed 2019 event, in the fully coupled PIC simulations of the CESM-LE projection were analyzed (Fig. 7). In general, the PIC simulations reproduced the observed circulation anomalies of EC precipitation deficiency connected to the El Niño Modoki-like SST anomaly over the tropical Pacific. During extreme EC drought years, the model-simulated SSTs showed statistically significant warm anomalies over the CEP with an anomalous warm center near the International Date Line and exhibited an El Niño Modoki-like pattern. Furthermore, a strong cyclonic anomaly occupied the WNP and brought significant northerly winds to EC. In the PIC simulations, the medians of 60-year sliding time window correlations of EMI with the EC area-mean meridional wind at 850 hPa and with precipitation were −0.45 and −0.32, respectively, and both were statistically significant at the 1% level. The agreement between the PIC simulations and observations further consolidates the connection between the El Niño Modoki-like SST anomaly and EC drought.

3.3. *Impact of anthropogenic warming*

Notably, the strongest EC precipitation deficiency in 2019 occurred simultaneously with the record-breaking high SATs (Fig. 1). Although extreme precipitation deficiencies and high temperature events do not necessarily occur at the same time (Sun and Yang, 2012; Lu et al., 2014), the concurrence of abnormally high temperatures with severe precipitation deficiencies might exacerbate local drought conditions due to the positive relationship between these factors (Lu et al., 2011; Li et al., 2018). Global warming and the associated increase in extreme temperatures substantially increase the chances of concurrent droughts and heat waves

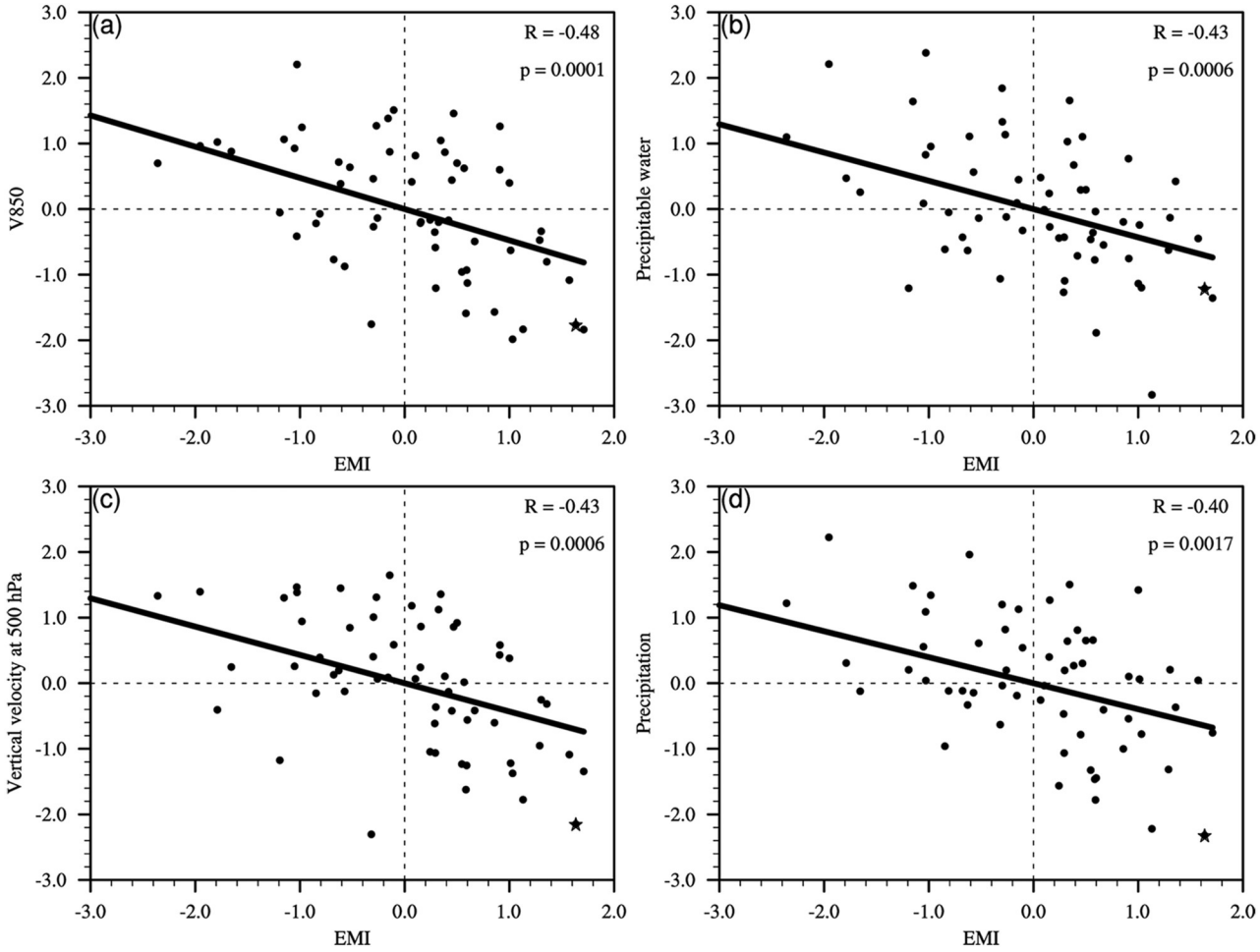

Fig. 6. Relationships between the EMI and observed variables related to the EC drought. Scatterplots between the standardized August–October mean EMI and (a) EC meridional wind at 850 hPa, (b) EC precipitable water, (c) EC sign-reversed pressure velocity at 500 hPa, and (d) EC precipitation from 1960 to 2019. Stars denote values for 2019. The least-squares regression lines are drawn in black, and the corresponding regression coefficients (R) are indicated in the top-right corner of the plots. The p value is the significance of R.

(AghaKouchak et al., 2014; Diffenbaugh et al., 2015; Williams et al., 2015; Ma et al., 2017). Thus, to understand the potential contribution of anthropogenic warming to the extreme EC drought in 2019, we compared the observed EMI, EC area-mean SAT and precipitation with CESM-LE simulations with only natural internal variability included and with simulations in which both climate change and natural internal variability were included.

Figure 8 shows the time series and 60-year sliding time window trends of the observed and model-simulated EMI, EC area-mean rainfall and SAT anomalies from August to October of 1920–2019. Here, the model ensemble mean highlights the externally forced signal, whereas the spread among the ensemble members reflects the unforced anomaly generated by the natural internal variability. The 2019 drought in EC occurred against a background of significant local warming. The observed EMI and EC area-mean rainfall anomalies show no significant trend from 1960–2019, but corresponding values in 2019 exhibit the second highest index value and lowest precipitation since 1960. The ensemble means of model simulated EMI and EC area-mean precipitation anomalies were small in contrast to the observation in 2019. The observed EMI and EC area-mean precipitation anomalies in 2019 fell within the large spread among the 40 CESM-LE members, and some individual members reproduced the amplitude of the observed high EMI value and precipitation deficiency percentage in EC. The observed EC area-mean SAT showed a significant warming trend of 0.86°C (60 yr)$^{-1}$, with a distinctive warm anomaly of 1.21°C in 2019 (Fig. 8e). The observed SAT anomaly in 2019 was within the range of the 40 CESM-LE ensemble members but was higher than the ensemble mean (an anomaly of 0.77°C). These results suggest that the external forcing encouraged surface warming from August to October of 2019 in EC, while the natural internal variability explains much of the high EMI and the precipitation deficit in EC.

Taking the PIC simulated internal variability as a surrogate for the natural internal variability in the real world (Kay et al., 2015; Ma et al., 2017; Swain et al., 2018), the

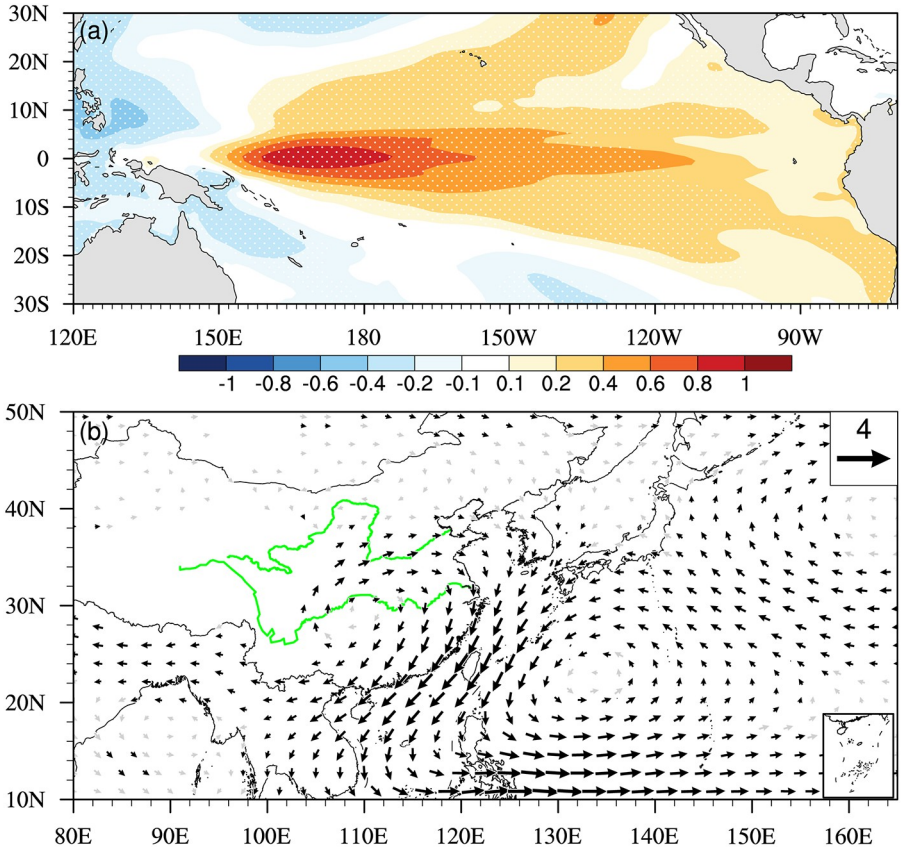

Fig. 7. Composite anomalies of (a) SST (units: °C) and (b) horizonal wind (units: m s^{-1}) at 850 hPa during EC extreme drought years (August–October precipitation meeting or falling below the 94-year return interval) in the PIC simulations of CESM1. Shading is stippled by white dots when they are significant at the 99% confidence level, and vectors are shown in black when they are significant at the 99% confidence level in at least one direction.

observed trends of EMI, EC area-mean SAT and precipitation were compared with those in the CESM-LE historical simulations and in the PIC simulations (Figs. 8b, d and f). This comparison shows that global warming favors the shifting of EMI long-term trends towards a warmer El Niño Modoki-like regime and the shifting of EC precipitation trends towards more severe precipitation deficiencies (Figs. 8b and d). However, no evidence suggests that it contributed to a significant increasing trend of EMI and a decreasing trend of rainfall in EC from 1960 to 2019. The observed trend in SAT from 1960 to 2019 was outside of the range of the 60-year sliding time window trend distribution in the PIC simulations, indicating that the warming SAT in EC cannot be explained by internal climate variability alone. Instead, the observed SAT trend [0.86°C (60 yr)$^{-1}$] was comparable to the ensemble mean trend [0.93°C (60 yr)$^{-1}$] from 1960–2019 and was within the range of the 60-year sliding time window trend distribution in the historical simulations. Such a result implies that the observed trend is consistent with the All-forcing simulations. Therefore, the significant warming trend in SAT over EC from 1960 to 2019 was very likely driven in part by anthropogenic forcing.

Did global warming contribute to the extreme EC drought in 2019? To reveal the impacts of global warming on the occurrence of severe drought events in EC like the 2019 drought, we compared the probability distribution functions (PDFs) of the simulated anomalies of EMI, EC area-mean precipitation and SAT from 1980 to 2019 with those in the PIC simulation. The period from 1980 to 2019 coincided with the start of a period of increased global warming, and since the 1980s, each successive decade has been warmer than any preceding decade since 1850 (WMO, 2020). There were clear indications of an increased probability of warmer El Niño Modoki-like regimes during the most recent four decades (Fig. 9a), which accompanied an increasing risk for more severe precipitation deficits in EC (Fig. 9c). There were also clear indications of an increased probability of warmer SAT in EC (Fig. 9e). In addition, in contrast to the PIC simulation, an increase in the occurrence frequency of concurrent dry and warm conditions from 1980 to 2019 was clear (Figs. 9b, d and f). There was no significant trend for the simulated August–October mean EMI and EC precipitation from 1960 to 2019, consistent with observations. However, the likelihood for high EMI and low EC precipitation extremes like that of 2019 significantly increased under anthropogenic warming. A mean of 2.56 (2.26–4.12) times and 2.22 (1.92–2.56) times increased frequency for high EMI and low EC precipitation extreme events analog-

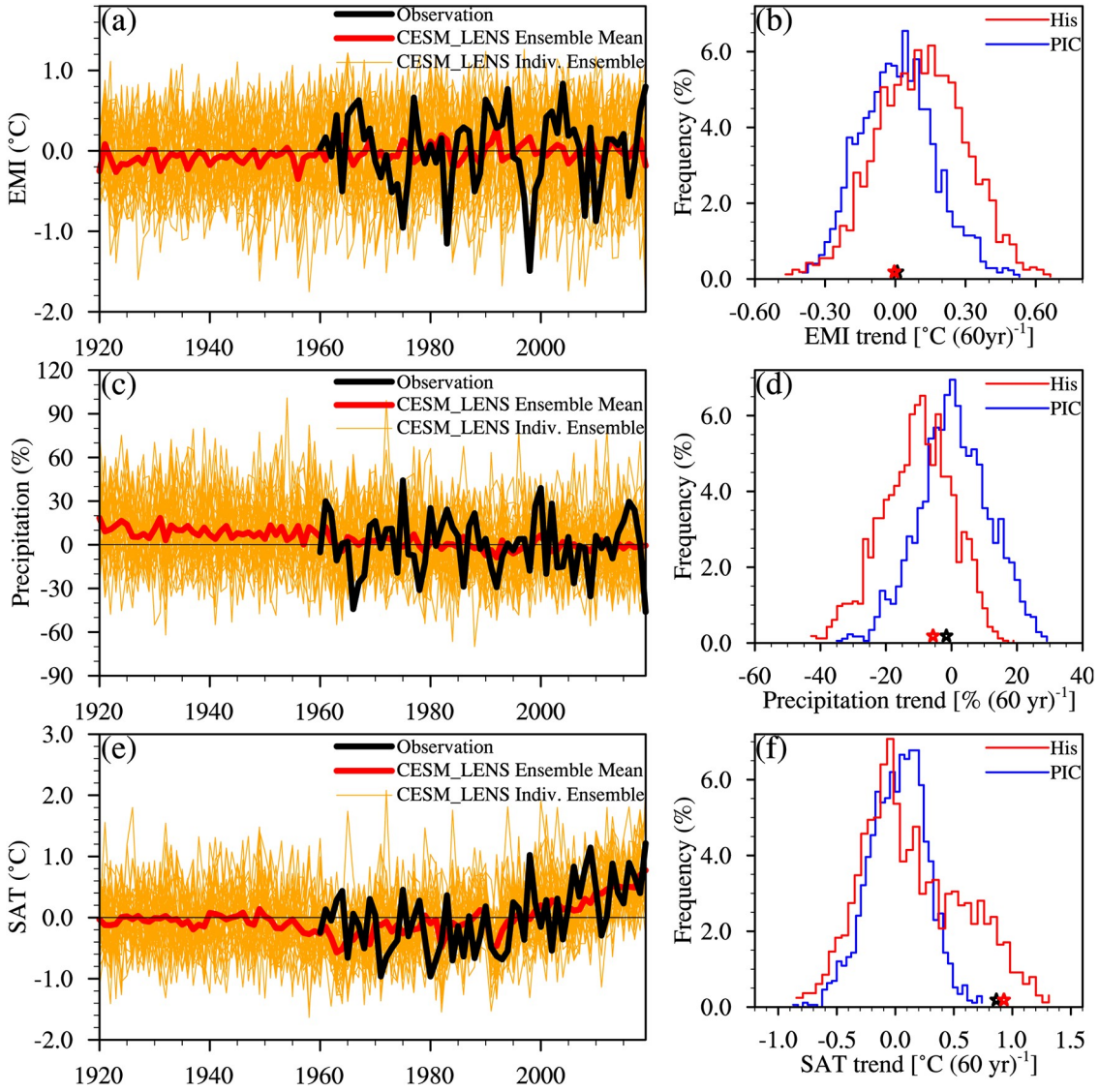

Fig. 8. Time series of August–October (a) EMI anomalies, (c) EC area-averaged SAT anomalies (unit: °C) and (e) EC area-averaged precipitation percentage anomalies (%) from 1920 to 2019. The black line depicts the observed anomalies, the dark red line depicts the ensemble mean anomalies from the 40-member CESM-LE runs, and the orange lines are individual ensemble members. Histograms of 60-year sliding trends of August–October mean (b) EMI [units: °C (60 yr)$^{-1}$], (d) EC area-averaged SAT [units: °C (60 yr)$^{-1}$] and (f) EC area-averaged precipitation percentage [% (60 yr)$^{-1}$]. The red curves show trends derived from the 40-member CESM-LE simulations from 1920 to 2019, the blue curves show trends derived from the PIC simulations, and the black (red) stars denote observed (40-member ensemble mean) trends from 1960 to 2019.

ous to that in 2019 can be attributed to anthropogenic forcing. EC high temperature events hotter than the observed 2019 event increased in frequency 2.14 (1.76–2.54) times under the influence of anthropogenic climate change. Meanwhile, the frequency of concurrent dry and hot extremes in EC analogous to the case in 2019 increased 2.34 (1.13–3.75) times due to anthropogenic climate forcing.

4. Summary and discussion

4.1. *Summary*

From August to October 2019, a particularly extreme drought event occurred in EC against a background of significant long-term warming. This study explored the mechanism that was probably responsible for the 2019 EC extreme drought, and the possible contributions from anthropogenic climate change, based on station precipitation and SAT data, JRA-55 reanalysis data and simulations provided by the CESM-LE projection. The results suggest that the naturally driven El Niño Modoki-like SST anomaly and anthropogenic warming strongly contributed to the 2019 EC drought and the concurrent high temperature.

The El Niño Modoki-like SST anomaly over the tropical Pacific likely led to a distinguishable August–October

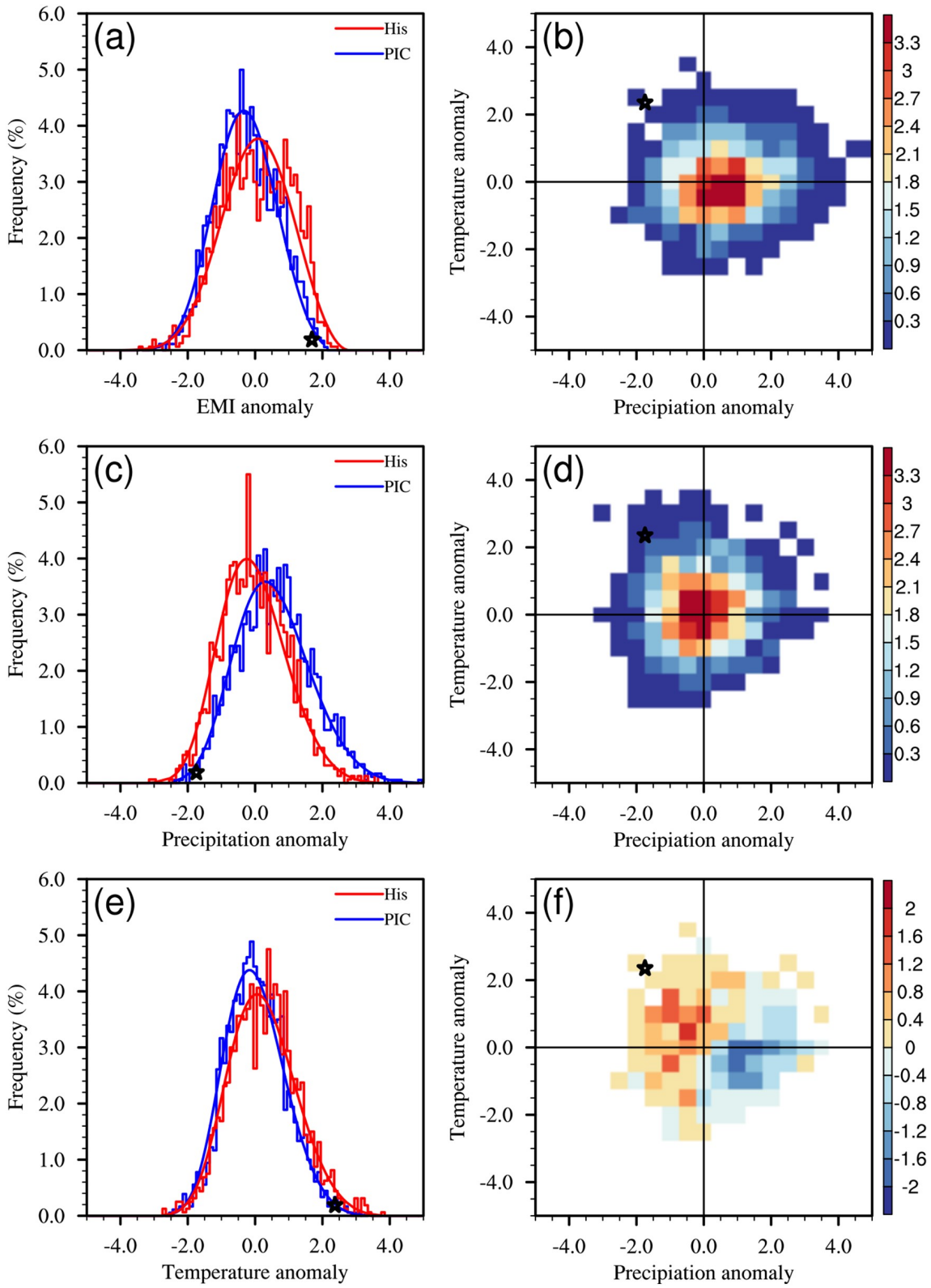

Fig. 9. Histograms (bars) and PDFs for the fitted GEV distribution of standardized August–October mean anomalies of the (a) EMI, (c) EC precipitation and (e) EC SAT derived from 40-member CESM-LE historical simulations from 1980 to 2019 (red) and the PIC simulations (blue). The joint PDF of the standardized August–October mean EC area-averaged anomalies of SAT and precipitation derived from (b) PIC simulations, (d) CESM-LE historical simulations from 1990 to 2019, and (f) the joint PDF difference between historical simulations from 1990 to 2019 and PIC simulations. Black stars denote the observed anomaly in 2019.

drought over EC by exciting an anomalous cyclone in the lower troposphere over the WNP, resulting in anomalous northerly winds over EC, thus inducing insufficient moisture concentrations and anomalous downward motion over EC and subsequently favoring severe precipitation deficiency and surface warming. The second highest El Niño Modoki-like SST from August to October since 1960, occurring in 2019, might have been one of the contributing drivers for the simultaneous severe drought over EC.

Analysis of CESM-LE simulations showed that natural internal variability accounted for the observed 2019 extreme El Niño Modoki-like warm SSTs in the tropical Pacific and the extreme precipitation deficits in EC. Long-term anthropogenic warming in EC from 1960 to 2019 was detectable and played an important role in accounting for the 2019 record-breaking high temperature in EC. Anthropogenic warming was found to yield an approximate twofold increase in the likelihood of EC extreme drought events such as the 2019 event for events showing extremely high temperature alone, low precipitation alone, or both. Therefore, the severe concurrent drought and high temperature event over EC in 2019 may have been caused by the combined impacts of the naturally driven El Niño Modoki-like SST anomaly and anthropogenic warming.

4.2. *Discussion*

In this study, based on the linear relationship between EMI and EC drought, it was suggested that the extreme warm El Niño Modoki-like SST in the tropical Pacific in 2019 played a crucial role in the simultaneous severe drought in EC. Previous studies report that the influences of warm and cold ENSO Modoki events on climate over East Asia are asymmetric (Feng and Li, 2011; Zhang et al., 2014; Li et al., 2019; Wang et al., 2020). Therefore, the possible asymmetric influence of the ENSO Modoki-like SST on the August–October droughts over EC deserves further study.

It has also been suggested that Indian Ocean Dipole (IOD) events have a close relationship with climate anomalies in East Asia (Zhang et al., 2017; Li and Zhao, 2019). The IOD has been shown to cause extremely hot and dry summers in South China by generating a Rossby wave train (Guan and Yamagata, 2003). An extreme positive IOD event occurred in 2019 and is linked with the pre-existing El Niño Modoki in the tropical Pacific (Doi et al., 2020). We examined the linear correlation of August–October EC precipitation with the IOD and found no significant linear correlation between them.

Acknowledgements. This study was jointly supported by the National Key R&D Program (Grant No. 2018YFC1505904), the National Natural Science Foundation of China (Grant Nos. 41830969 and 41705052) and the Basic Scientific Research and Operation Foundation of CAMS (Grant No. 2018Z006).

REFERENCES

Agha Kouchak, A., L. Y. Cheng, O. Mazdiyasni, and A. Farahmand, 2014: Global warming and changes in risk of concurrent climate extremes: Insights from the 2014 California drought. *Geophys. Res. Lett.*, **41**, 8847–8852, https://doi.org/10.1002/2014GL062308.

Ashok, K., S. K. Behera, S. A. Rao, H. Y. Weng, and T. Yamagata, 2007: El Niño Modoki and its possible teleconnection. *J. Geophys. Res.*, **112**, C11007, https://doi.org/10.1029/2006JC003798.

Coumou, D., and S. Rahmstorf, 2012: A decade of weather extremes. *Nature Climate Change*, **2**(7), 491–496, https://doi.org/10.1038/nclimate1452.

Dai, A. G., 2011: Drought under global warming: A review. *Wiley Interdisciplinary Reviews: Climate Change*, **2**(1), 45–65, https://doi.org/10.1002/wcc.81.

Dai, A. G., 2013: Increasing drought under global warming in observations and models. *Nature Climate Change*, **3**(1), 52–58, https://doi.org/10.1038/nclimate1633.

Diffenbaugh, N. S., D. L. Swain, and D. Touma, 2015: Anthropogenic warming has increased drought risk in California. *Proceedings of the National Academy of Sciences of the United States of America*, **112**, 3931–3936, https://doi.org/10.1073/pnas.1422385112.

Doi, T., S. K. Behera, S. K., and T. Yamagata, 2020: Predictability of the super IOD event in 2019 and its link with El Niño Modoki. *Geophys. Res. Lett.*, **47**, e2019GL086713, https://doi.org/10.1029/2019GL086713.

Feng, J., and J. P. Li, 2011: Influence of El Niño Modoki on spring rainfall over south China. *J. Geophys. Res.*, **116**, D13102, https://doi.org/10.1029/2010JD015160.

Feng, J., J. P. Li, F. Zheng, F. Xie, and C. Sun, 2016: Contrasting impacts of developing phases of two types of El Niño on Southern China rainfall. *J. Meteor. Soc. Japan*, **94**(4), 359–370, https://doi.org/10.2151/jmsj.2016-019.

Feng, J., J. P. Li, J. L. Zhu, H. Liao, and Y. Yang, 2017: Simulated contrasting influences of two La Niña Modoki events on aerosol concentrations over eastern China. *J. Geophys. Res.*, **122**, 2734–2749, https://doi.org/10.1002/2016JD026175.

Feng, L., T. Li, and W. D. Yu, 2014: Cause of severe droughts in Southwest China during 1951–2010. *Climate Dyn.*, **43**(7–8), 2033–2042, https://doi.org/10.1007/s00382-013-2026-z.

Gao, T., M. Luo, N. C. Lau, and T. O. Chan, 2020: Spatially distinct effects of two El Niño types on summer heat extremes in China. *Geophys. Res. Lett.*, **47**, e2020GL086982, https://doi.org/10.1029/2020GL086982.

Guan, Z. Y., and T. Yamagata, 2003: The unusual summer of 1994 in East Asia: IOD teleconnections. *Geophys. Res. Lett.*, **30**(10), 1544, https://doi.org/10.1029/2002GL016831.

Ham, Y. G., J. S. Kug, and I. S. Kang, 2007: Role of moist energy advection in formulating anomalous Walker Circulation associated with El Niño. *J. Geophys. Res.*, **112**, D24105, https://doi.org/10.1029/2007JD008744.

Hoell, A., J. Perlwitz, C. Dewes, K. Wolter, I. Rangwala, X. W. Quan, and J. Eischeid, 2019: Anthropogenic contributions to the intensity of the 2017 United States northern great plains drought. *Bull. Amer. Meteor. Soc.*, **100**(1), S19–S24, https://doi.org/10.1175/BAMS-D-18-0127.1.

Huang, B. Y., and Coauthors, 2017: NOAA Extended Reconstructed Sea Surface Temperature (ERSST), Version 5. [indicate subset used]. NOAA National Centers for Environmental Information, https://doi.org/10.7289/V5T72FNM.

Huang, J. P., H. P. Yu, X. D. Guan, G. Y. Wang, and R. X. Guo,

2016: Accelerated dryland expansion under climate change. *Nature Climate Change*, **6**, 166–171, https://doi.org/10.1038/nclimate2837.

Huang, T., L. G. Xu, and H. X. Fan, 2019: Drought characteristics and its response to the global climate variability in the Yangtze River Basin, China. *Water*, **11**(1), 13, https://doi.org/10.3390/w11010013.

Jin, D. C., Z. Y. Guan, and W. Y. Tang, 2013: The extreme drought event during winter-spring of 2011 in East China: Combined influences of teleconnection in midhigh latitudes and thermal forcing in maritime continent region. *J. Climate*, **26**(20), 8210–8222, https://doi.org/10.1175/JCLI-D-12-00652.1.

Kay, J. E., and Coauthors, 2015: The Community Earth System Model (CESM) large ensemble project: A community resource for studying climate change in the presence of internal climate variability. *Bull. Amer. Meteor. Soc.*, **96**, 1333–1349, https://doi.org/10.1175/BAMS-D-13-00255.1.

Kobayashi, S., and Coauthors, 2015: The JRA-55 Reanalysis: General specifications and basic characteristics. *J. Meteor. Soc. Japan*, **93**, 5–48, https://doi.org/10.2151/jmsj.2015-001.

Lewis, S. L., P. M., Brando, O. L. Phillips, G. M. F. van der Heijden, and D. Nepstad, 2011: The 2010 amazon drought. *Science*, **331**(6017), 554, https://doi.org/10.1126/science.1200807.

Li, C. X., and T. B. Zhao, 2019: Seasonal responses of precipitation in China to El Niño and positive Indian Ocean Dipole modes. *Atmosphere*, **10**, 372, https://doi.org/10.3390/atmos10070372.

Li, H. X., H. P. Chen, H. J. Wang, J. Q. Sun, and J. H. Ma, 2018: Can Barents sea ice decline in spring enhance summer hot drought events over northeastern China? *J. Climate*, **31**(12), 4705–4725, https://doi.org/10.1175/JCLI-D-17-0429.1.

Li, Y, B. S. Ma, J. Feng, and Y. Lu, 2019: Influence of the strongest central Pacific El Niño-Southern Oscillation events on the precipitation in eastern China. *International Journal of Climatology*, **39**, 3076–3090, https://doi.org/10.1002/joc.6004.

Lott, F. C., N. Christidis, and P. A. Stott, 2013: Can the 2011 East African drought be attributed to human-induced climate change? Geophys *Res. Lett.*, **40**, 1177–1181, https://doi.org/10.1002/grl.50235.

Lu, E., and Coauthors, 2014: The atmospheric anomalies associated with the drought over the Yangtze River basin during spring 2011. *J. Geophys. Res.*, **119**, 5881–5894, https://doi.org/10.1002/2014JD021558.

Lu, E., Y. L. Luo, R. H. Zhang, Q. X. Wu, and L. P. Liu, 2011: Regional atmospheric anomalies responsible for the 2009-2010 severe drought in China. *J. Geophys. Res.*, **116**, D21114, https://doi.org/10.1029/2011JD015706.

Ma, S. M., T. J. Zhou, O. Angélil, and H. Shiogama, 2017: Increased chances of drought in southeastern periphery of the Tibetan Plateau induced by anthropogenic warming. *J. Climate*, **30**(16), 6543–6560, https://doi.org/10.1175/JCLI-D-16-0636.1.

Ren, H. L., B. Lu, J. H. Wan, B. Tian, and P. Q. Zhang, 2018: Identification standard for ENSO events and its application to climate monitoring and prediction in China. *Journal of Meteorological Research*, **32**(6), 923–936, https://doi.org/10.1007/s13351-018-8078-6.

Sternberg, T., 2011: Regional drought has a global impact. *Nature*, **472**(7342), 169, https://doi.org/10.1038/472169d.

Sun, C. H., and S. Yang, 2012: Persistent severe drought in southern China during winter-spring 2011: Large-scale circulation patterns and possible impacting factors. *J. Geophys. Res.*, **117**, D10112, https://doi.org/10.1029/2012JD017500.

Sun, F. Y., A. Mejia, P. Zeng, and Y. Che, 2019: Projecting meteorological, hydrological and agricultural droughts for the Yangtze River basin. *Science of the Total Environment*, **696**, 134076, https://doi.org/10.1016/j.scitotenv.2019.134076.

Swain, D. L., B. Langenbrunner, J. D. Neelin, and A. Hall, 2018: Increasing precipitation volatility in twenty-first-century California. *Nature Climate Change*, **8**(5), 427–433, https://doi.org/10.1038/s41558-018-0140-y.

Trenberth, K. E., 2011: Changes in precipitation with climate change. *Climate Research*, **47**, 123–138, https://doi.org/10.3354/cr00953.

Trenberth, K. E., A. G. Dai, G. van der Schrier, P. D. Jones, J. Barichivich, K. R. Briffa, and J. Sheffield, 2014: Global warming and changes in drought. *Nature Climate Change*, **4**, 17–22, https://doi.org/10.1038/nclimate2067.

Trenberth, K. E., J. T. Fasullo, and T. G. Shepherd, 2015: Attribution of climate extreme events. *Nature Climate Change*, **5**(8), 725–730, https://doi.org/10.1038/nclimate2657.

Wang, D., A. H. Wang, L. L. Xu, and X. H. Kong, 2020: The linkage between two types of El Niño events and summer streamflow over the Yellow and Yangtze River Basins. *Adv. Atmos. Sci.*, **37**, 160–172, https://doi.org/10.1007/s00376-019-9049-2.

Wang, L., and W. Chen, 2014: A CMIP5 multimodel projection of future temperature, precipitation, and climatological drought in China. *International Journal of Climatology*, **34**(6), 2059–2078, https://doi.org/10.1002/joc.3822.

Wang, L., W. Chen, W. Zhou, and G. Huang, 2015: Teleconnected influence of tropical Northwest Pacific sea surface temperature on interannual variability of autumn precipitation in Southwest China. *Climate Dyn.*, **45**(9-10), 2527–2539, https://doi.org/10.1007/s00382-015-2490-8.

Williams, A. P., R. Seager, J. T. Abatzoglou, B. I. Cook, J. E. Smerdon, and E. R. Cook, 2015: Contribution of anthropogenic warming to California drought during 2012–2014. *Geophys. Res. Lett.*, **42**, 6819–6828, https://doi.org/10.1002/2015GL064924.

WMO, 2020: WMO Statement on the State of the Global Climate in 2019. [Available online from https://library.wmo.int/doc_num.php?explnum_id=10211]

Wu, B., T. J. Zhou, and T. Li, 2017: Atmospheric dynamic and thermodynamic processes driving the Western North Pacific anomalous anticyclone during El Niño. Part I: Maintenance mechanisms. *J. Climate*, **30**, 9621–9635, https://doi.org/10.1175/JCLI-D-16-0489.1.

Wu, Z. W., J. P. Li, J. H. He, and Z. H. Jiang, 2006: Occurrence of droughts and floods during the normal summer monsoons in the mid- and lower reaches of the Yangtze River. *Geophys. Res. Lett.*, **33**, L05813, https://doi.org/10.1029/2005GL024487.

Yang, J., D. Y. Gong, W. S. Wang, M. Hu, and R. Mao, 2012: Extreme drought event of 2009/2010 over southwestern China. *Meteorol. Acs.*, **115**(3–4), 173–184, https://doi.org/10.1007/s00703-011-0172-6.

Yang, S. Y., B. Y. Wu, R. H. Zhang, and S. W. Zhou, 2013: Relationship between an abrupt drought-flood transition over mid-low reaches of the Yangtze River in 2011 and the intraseasonal oscillation over mid-high latitudes of East

Asia. *Acta Meteorologica Sinica*, **27**(2), 129–143, https://doi.org/10.1007/s13351-013-0201-0.

Yu, J. Y., X. Wang, S. Yang, H. Paek, and M. Y. Chen, 2017: The changing El Niño-Southern Oscillation and associated climate extremes. *Climate Extremes: Patterns and Mechanisms*, Wang et al., Eds., American Geophysical Union, 1-38, https://doi.org/10.1002/9781119068020.ch1.

Yu, M. X., Q. F. Li, M. J. Hayes, M. D. Svoboda, and R. R. Heim, 2014: Are droughts becoming more frequent or severe in China based on the standardized precipitation evapotranspiration index: 1951-2010? *International Journal of Climatology*, **34**(3), 545–558, https://doi.org/10.1002/joc.3701.

Yuan, Y., and S. Yang, 2012: Impacts of different types of El Niño on the East Asian climate: focus on ENSO cycles. *J. Climate*, **25**, 7702–7722, https://doi.org/10.1175/JCLI-D-11-00576.1.

Zeng, D. W., X. Yuan, and J. K. Roundy, 2019: Effect of teleconnected land-atmosphere coupling on Northeast China persistent drought in spring-summer of 2017. *J. Climate*, **32**(21), 7403–7420, https://doi.org/10.1175/JCLI-D-19-0175.1.

Zhang, D., Q. Zhang, A. D. Werner, and X. M. Liu, 2016: GRACE-Based hydrological drought evaluation of the Yangtze River Basin, China. *Journal of Hydrometeorology*, **17**, 811–828, https://doi.org/10.1175/JHM-D-15-0084.1.

Zhang, L., F. Sielmann, K. Fraedrich, and X. F. Zhi, 2017: Atmospheric response to Indian Ocean Dipole forcing: Changes of Southeast China winter precipitation under global warming. *Climate Dyn.*, **48**, 1467–1482, https://doi.org/10.1007/s00382-016-3152-1.

Zhang, L., P. L. Wu, T. J. Zhou, and C. Xiao, 2018: ENSO transition from La Niña to El Niño drives prolonged spring-summer drought over north China. *J. Climate*, **31**(9), 3509–3523, https://doi.org/10.1175/JCLI-D-17-0440.1.

Zhang, L. X., and T. J. Zhou, 2015: Drought over East Asia: A review. *J. Climate*, **28**, 3375–3399, https://doi.org/10.1175/JCLI-D-14-00259.1.

Zhang, W. J., F. F. Jin, J. P. Li, and H. L. Ren, 2011: Contrasting impacts of two-type El Niño over the western North Pacific during boreal autumn. *J. Meteor. Soc. Japan*, **89**(5), 563–569, https://doi.org/10.2151/jmsj.2011-510.

Zhang, W. J., F. F. Jin, J. X. Zhao, L. Qi, and H. L. Ren, 2013: The possible influence of a nonconventional El Niño on the severe autumn drought of 2009 in Southwest China. *J. Climate*, **26**(21), 8392–8405, https://doi.org/10.1175/JCLI-D-12-00851.1.

Zhang, W. J., F. F. Jin, and A. Turner, 2014: Increasing autumn drought over southern China associated with ENSO regime shift. *Geophys. Res. Lett.*, **41**, 4020–4026, https://doi.org/10.1002/2014GL060130.